Current Biology, Volume *32*

Supplemental Information

Optic flow in the natural habitats of zebrafish supports spatial biases in visual self-motion estimation

Emma Alexander, Lanya T. Cai, Sabrina Fuchs, Tim C. Hladnik, Yue Zhang, Venkatesh Subramanian, Nicholas C. Guilbeault, Chinnian Vijayakumar, Muthukumarasamy Arunachalam, Scott A. Juntti, Tod R. Thiele, Aristides B. Arrenberg, and Emily A. Cooper

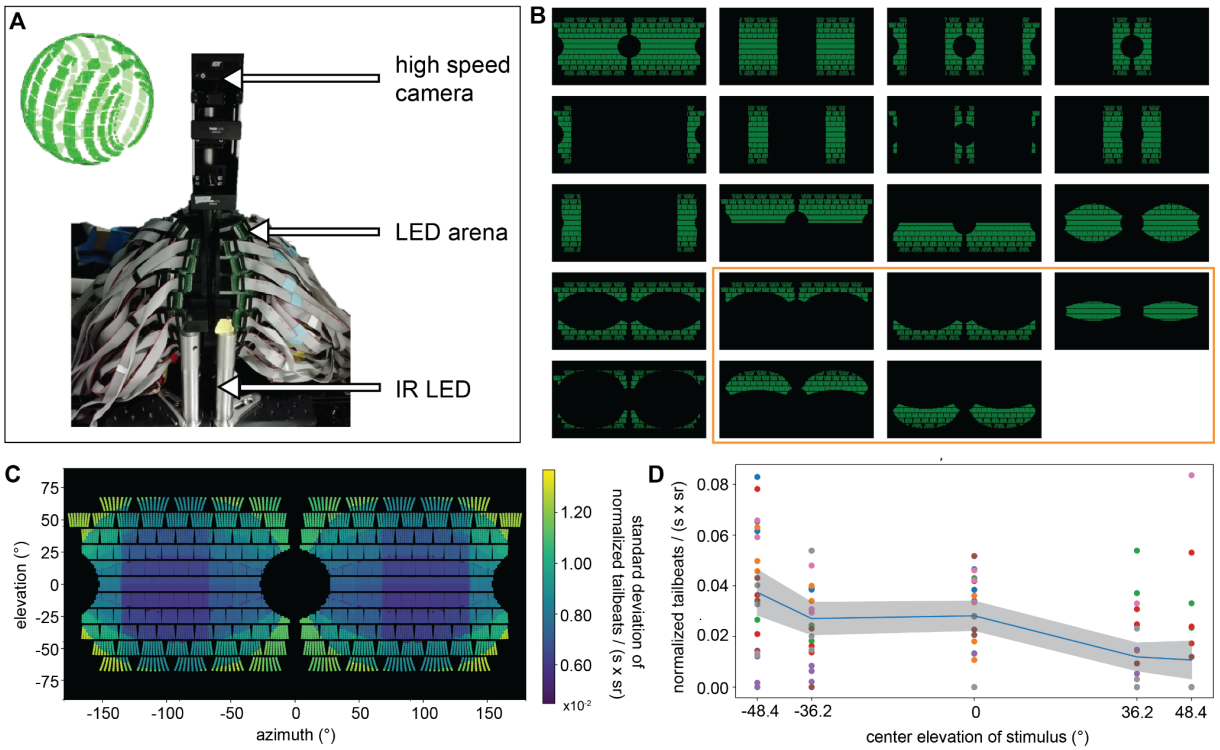

Figure S1: Spherical stimulation arena for behavioral experiment and stimulus spatial patterns. Related to Figure 3.

(A) The outside of the behavioral arena shows spherically arranged LED tiles. Fish were positioned in the arena and illuminated by an infrared (IR) LED, while a high speed camera imaged the behavior from above. A sample frame of the striped stimulus pattern is shown in the top left for full sphere illumination. (B) The 19 spatial regions where backward motion was presented to the fish while OMR was measured. In the black regions covered by LEDs, a stationary pattern was presented in order to avoid abrupt luminance changes when the motion phases were changed. Subplots show full azimuth and elevation ranges as in panel C. (C) Optomotor responses showed variations from fish to fish and from trial to trial. Here we show the standard deviation across fish for the overall responses shown in Figure 3. (D) Responses for each trial are shown for eight individual fish (different colors), showing variation across trials and individuals. The mean response of each fish was combined into a mean (blue line) ± standard error (grey region), where the grey region appears in blue in the graphical abstract as a summary of the elevation-dependent behavioral response. Note that the fish shown in green only underwent 2 trials due to a conflict between experiment time and the circadian rhythm of the fish; the mean of these 2 trials was considered with equal weight to the mean across 3 trials for all other individuals. The five elevation-isolating stimulus regions used in this analysis are bounded in orange in panel B.

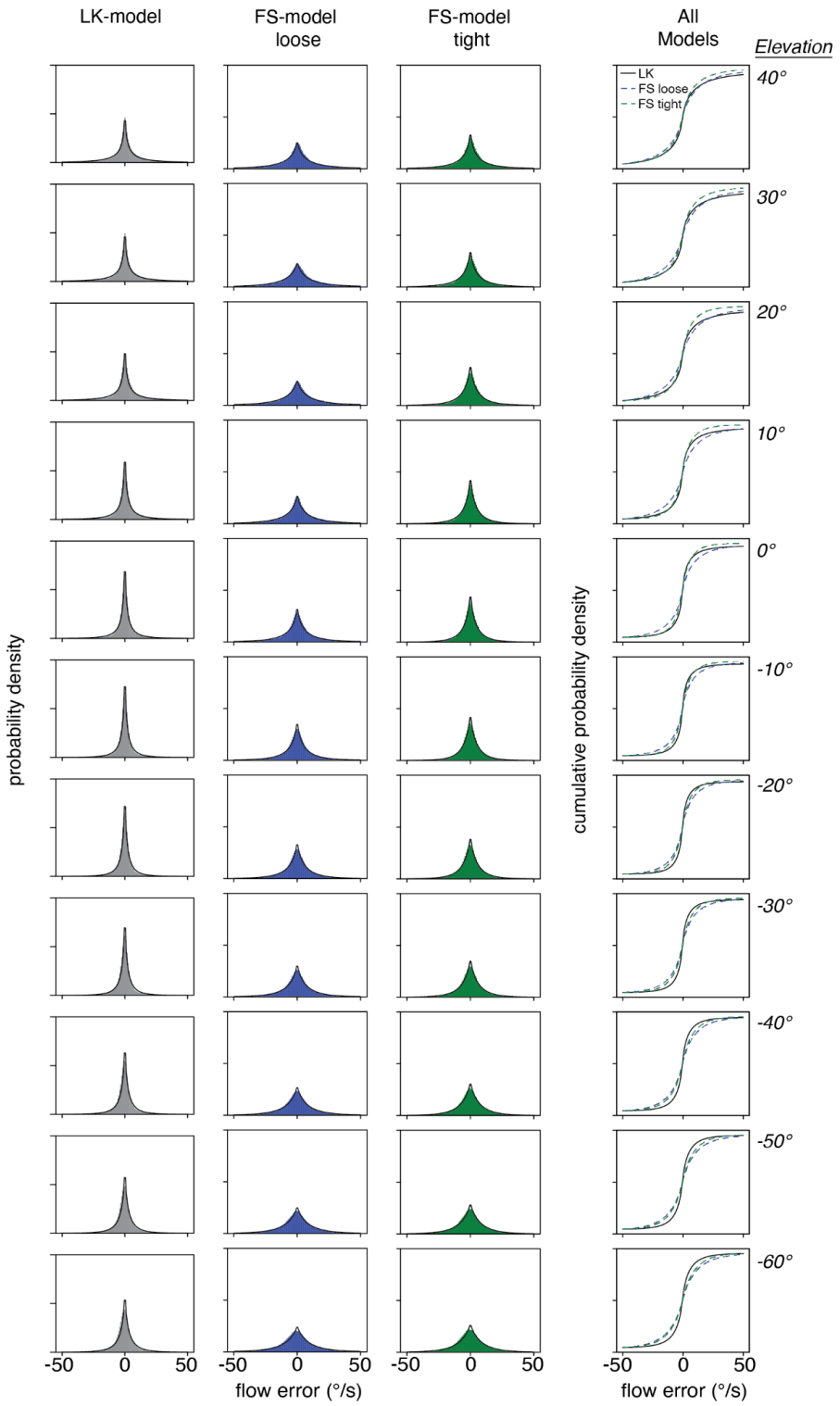

Figure S2: Environmental motion noise by elevation in the native habitat of the zebrafish. Related to Figure 4.

Errors in individual optic flow estimates for rotation show systematic changes across elevation. In the left three columns, histograms of errors from three optic flow calculation methods are shown along with maximum likelihood estimates of a generalized Gaussian. Histograms are normalized to probability density and all panel ordinates go from 0 to 0.2. The fits for each model are compared in the right column as cumulative probability densities and parameters of the fits are listed in Table S4. The LK method (black) results in systematically lower errors than the FS method with a loose contrast threshold set to roughly match the LK sparsities (blue). Tightening the contrast threshold (green) partially recovers accuracy at the cost of higher sparsity (see Figure 4). Elevation trends are similar across all three methods.

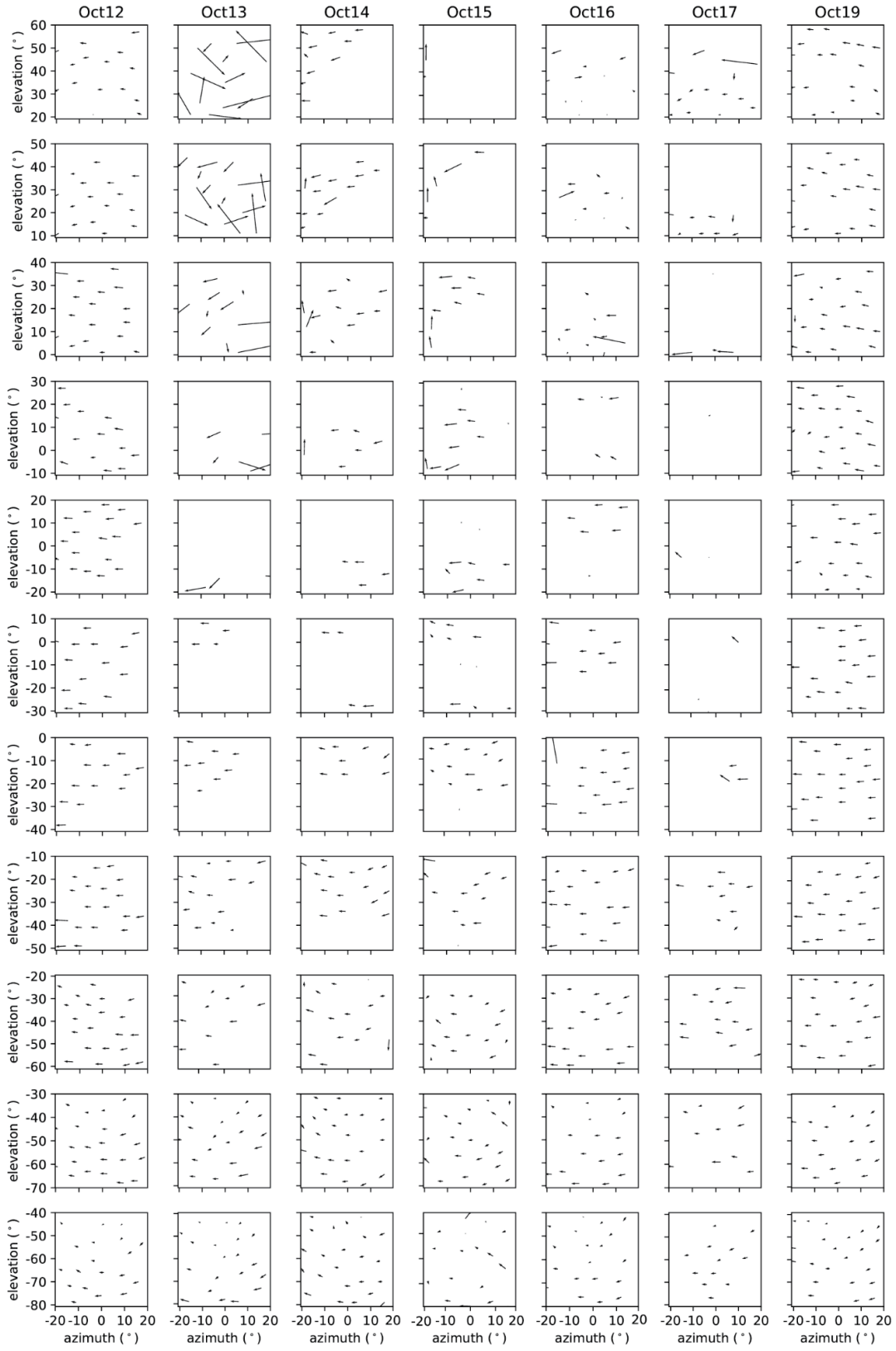

Figure S3. Example local optical flow by elevation for each field site. Related to Figure 4.

For each field site (column), the LK-based optic flow at one frame at each sampled elevation (row) is shown for a 40° by 40° area during a camera rotation. Elevations go from upper to lower visual field as indicated in Figure S2.

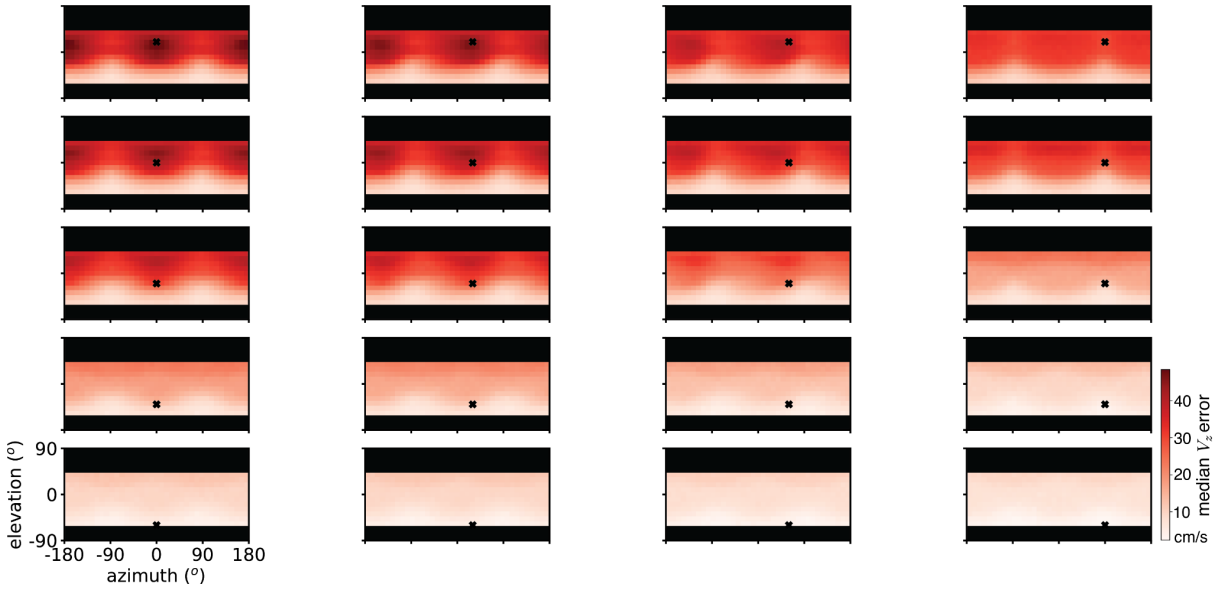

Figure S4: Forward speed (V_z) estimation error for simulated saccadic swimming for each base RF location. Related to Figure 5.

Median self-motion estimation error for forward speed is shown for each base receptive field location, indicated with an x. Rows in this figure correspond to colors in Figure 5 (base RF elevation) and columns correspond to line thickness (base RF azimuth). The bottom right plot is included (on a magnified color scale) in Figure 5A.

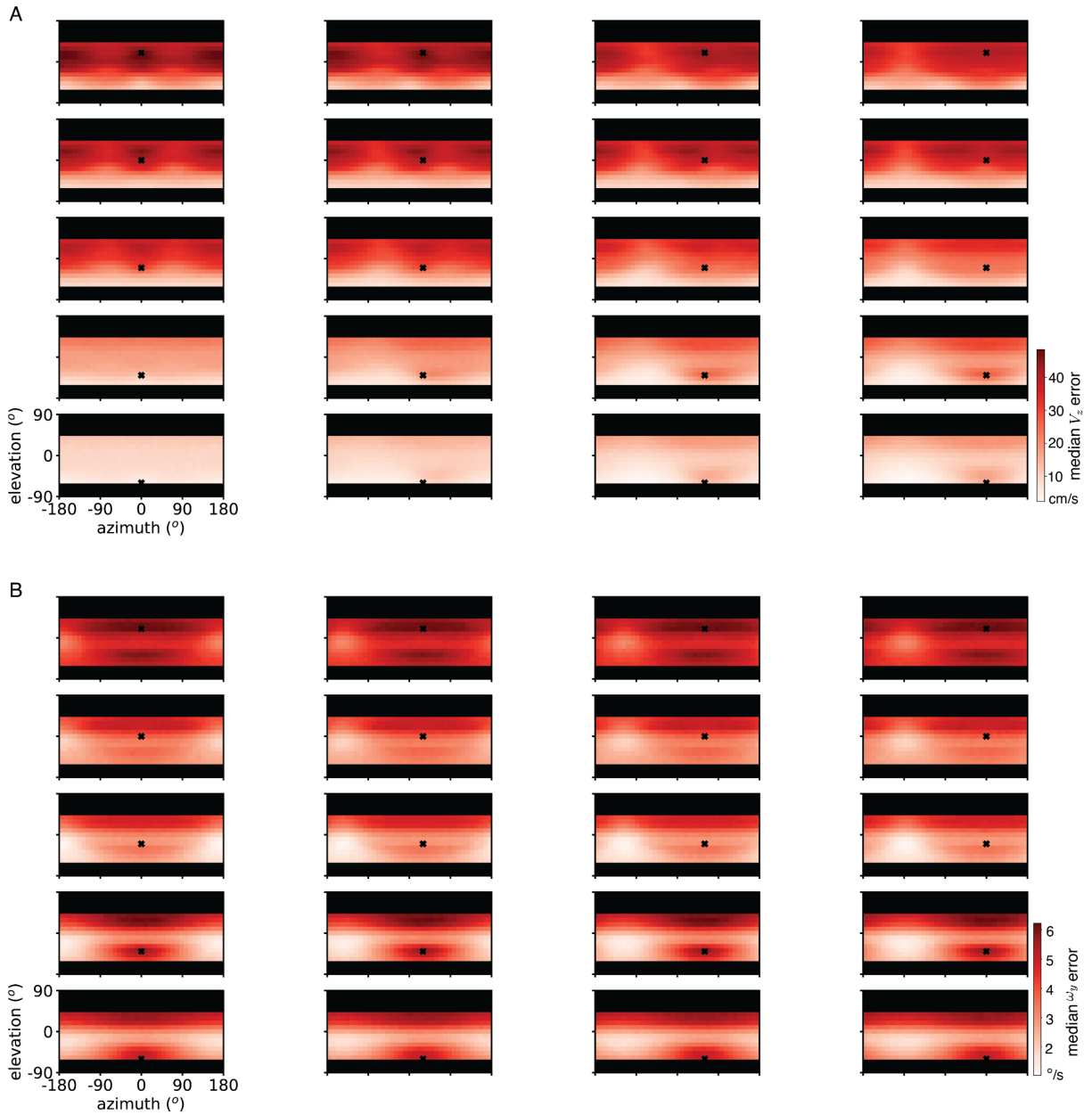

Figure S5: Forward speed (V_z) and rotation (ω_y) estimation error for simulated compound swimming. Related to Figure 5.

Median forward speed (A) and rotation (B) error is shown for each base receptive field, indicated with an x. Data are plotted in the same format as Figure S4. The bottom right plot in panel A and the middle right panel in B are included (on a magnified color scale) in Figure 5B.

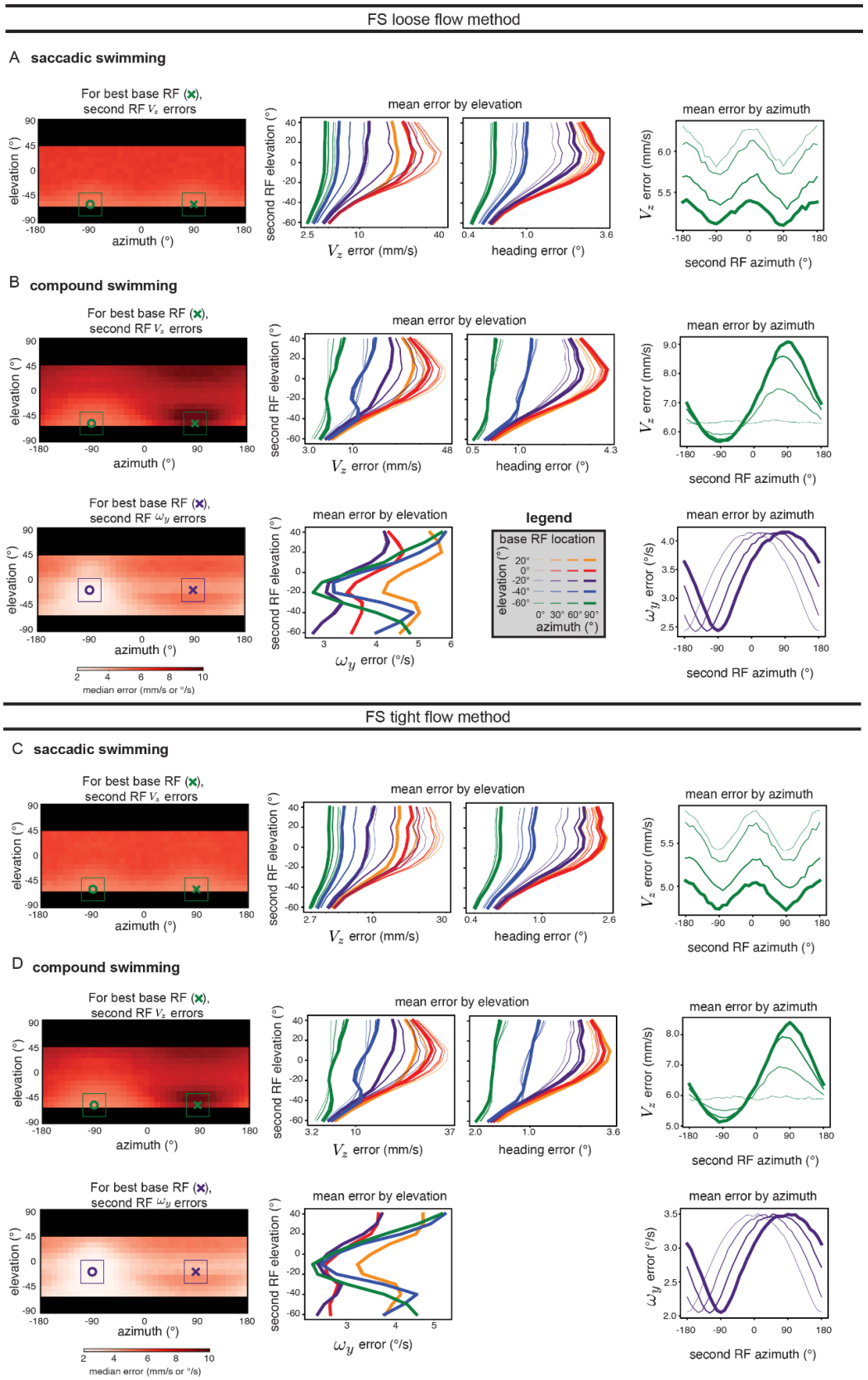

Figure S6: Simulated swimming results hold across noise models. Related to Figure 5.

The simulations shown in Figure 5 are repeated for FS-based noise models with loose (A,B) and tight (C,D) restrictions on luminance gradient magnitude. Results are slightly worse under these models, but trends in optimal sampling locations hold.

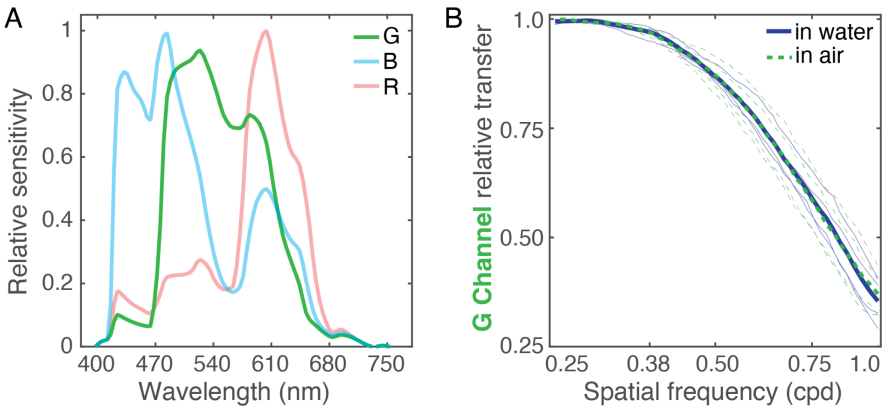

Figure S7: Camera sensitivity: wavelength and spatial frequency. Related to Figure 4.

(A) The average spectral sensitivity of the cameras in one device (including contributions of the dive case, lens, sensor, and white balance). The second device had very similar sensitivity. R, G, and B denote the red, green, and blue channels, respectively. (B) The average (thick lines) and individual (thin lines) modulation transfer functions of the green (G) channel measured for each camera (4 total) in air and water within the spatial frequency range of interest (up to 1.0 cpd).

Site	Date (2019)	Location	GPS Coordinates
1	October 12	Bhalia	26° 00' 01.0" N, 91° 29' 22.7" E
2	October 13	Mirza-Rajapara Road	25° 52' 28.2" N, 91° 27' 18.4" E
3	October 14	Khalihamari	26° 18' 44.7" N, 91° 28' 30.0" E
4	October 15	Tumprop	26° 03' 07.1" N, 92° 25' 52.5" E
5	October 16	Pagladia River, Bhutan Border	26° 48' 55.0" N, 91° 24' 55.6" E
6	October 17	Niz Udalguri	26° 46' 25.4" N, 92° 07' 22.7" E
7	October 19	Goldighala	26° 17' 01.0" N, 91° 26' 59.8" E

Table S1: Temporal and geographic data for field recording sites. Related to Figure 4.

Collection dates were two weeks after major rainfall, so water clarity in the dataset is likely typical for non-monsoon conditions at these sites. Note that due to variation in the camera mounting, we time-reversed some videos to preserve the direction of translation and rotation. In the public dataset, these videos are indicated with negative frame numbers. Details of trajectory reversals can be found in the documentation associated with the public code.

Velocity	# of sites	# of frames per site
40 mm/s forward	7	400
40 mm/s sideways	7	400
40 mm/s diagonal	7	400
60 mm/s forward	7	400
60 mm/s sideways	7	400
60 mm/s diagonal	7	400
20°/s clockwise	7	400
50°/s clockwise	7	400
40 mm/s forward + 15°/s	3	400
40 mm/s forward + 45°/s	3	350
60 mm/s forward + 20°/s	3	400
60 mm/s forward + 50°/s	3	300

Table S2: Optic flow samples from the native habitat of the larval zebrafish. Related to Figure 4.

For each trajectory, up to 400 image pairs are considered, each separated by a time step of 50 ms. Most trajectories are sampled at all 7 sites but combined rotation and translation trajectories were not available at all sites, so only sites 3, 4, and 7 are included here.

Parameter	Insta1	
	Camera 1	*Camera 2*
Mapping coeff (a)	[463.5480 -0.0010 0 0]	[460.1266 -0.0010 0 0]
Stretch matrix (α)	[1.0022 0.0063 -0.0054 1.0000]	[1.0020 0.0053 -0.0044 1.0000]
distortion center (u_c, v_c)	[750.1819 745.2155]	[754.3002 750.2068]
Ave. error (pixels)	0.98	1.01
	Insta 2	
	Camera 1	*Camera 2*
Mapping coeff (a)	[468.5216 -0.0012 0 0]	[466.4758 -0.0012 0 0]
Stretch matrix (α)	[0.9998 -0.0003 -0.0006 1.0000]	[0.9982 0.0018 -0.0030 1.0000]
distortion center (u_c, v_c)	[751.1434 749.6796]	[749.3261 746.8164]
Ave. error (pixels)	1.00	0.85

Table S3. Camera calibration parameters. Related to Figure 4.

Estimated camera intrinsics for each device (Insta1, Insta2) and camera (cam1, cam2). Parameters are provided for the green camera channel. Parameters include: mapping coefficients *a*, stretch matrix α, and distortion center [u_c, v_c]. Average reprojection errors in pixels were calculated for a large number of points spread over the cameras' visual field. Parameters refer to the OpenCV fish eye camera model described in Scaramuzza et al. (2006) and implemented in Matlab.

Elevation (°)	**40**	**30**	**20**	**10**	**0**	**-10**	**-20**	**-30**	**-40**	**-50**	**-60**
					LK						
Width (σ)	.945	.759	.841	.720	.767	.979	1.18	1.35	1.70	2.19	2.36
Shape (β)	.423	.400	.417	.433	.468	.519	.551	.569	.593	.629	.627
Sparsity (%)	61.3	62.5	63.7	67.0	64.9	57.2	48.4	39.8	33.2	30.2	27.9
					FS, loose threshold						
Width (σ)	5.80	7.41	7.45	5.85	4.60	4.55	5.33	6.21	7.42	8.12	8.71
Shape (β)	.623	.678	.696	.650	.635	.676	.723	7.49	.783	.800	.816
Sparsity (%)	67.3	64.4	61.3	61.7	59.8	57.2	43.2	33.8	26.9	23.9	23.5
					FS, tight threshold						
Width (σ)	4.00	4.33	4.60	3.99	3.93	3.57	5.08	5.72	6.75	7.61	8.32
Shape (β)	.601	.638	.712	.716	.735	.793	.800	.811	.825	.851	.863
Sparsity (%)	78.4	78.3	79.6	78.9	75.6	68.8	58.6	51.4	44.9	40.4	37.8

Table S4: Environmental motion noise model parameters by elevation for simulation of realistic optic flow fields in natural habitats of the zebrafish. Related to Figure 4.

Width and shape parameters reflect the generalized Gaussian fits to the data in Figure S2 for three flow calculation methods. Sparsity indicates the percentage of possible flow vectors that were recovered with each method.